JOURNAL OF MAGNETIC RESONANCE **128,** 199–206 (1997)
ARTICLE NO. MN971234

Pulsed ENDOR Spectroscopy at Large Thermal Spin Polarizations and the Absolute Sign of the Hyperfine Interaction

M. T. Bennebroek and J. Schmidt

Huygens Laboratory, Leiden University, P.O. Box 9504, 2300 RA Leiden, The Netherlands

Received March 7, 1997

It is shown that in pulsed Mims-type ENDOR experiments performed at 95 GHz and 1.2 K the sign of the ENDOR signal can be positive, corresponding to an increase of the stimulated echo intensity, as well as negative, corresponding to a decrease of the stimulated echo. The positive ''anomalous'' sign is not observed at conventional EPR frequencies. It is explained that the effect arises through spin–lattice relaxation in the situation of large thermal spin polarizations and that it allows the determination of the absolute sign of the hyperfine interaction.

1. INTRODUCTION

Electron nuclear double resonance (ENDOR) spectroscopy is widely used for the measurement of small hyperfine and nuclear quadrupole interactions that are not resolved in electron paramagnetic resonance (EPR) spectra. In the original continuous wave (CW) ENDOR technique, introduced by Feher in 1956 (*1*), an EPR transition is partially saturated with an intense CW microwave field. A second radiofrequency field induces nuclear magnetic resonance (NMR) transitions which are detected as a desaturation of the EPR signal. The CW ENDOR effect depends on the delicate balance between the effective electron and nuclear spin–lattice relaxation rates which mostly restrict the observation of the CW ENDOR signal to a narrow temperature range. In contrast, in pulsed ENDOR the applied pulse sequences can usually be made short compared to the spin–lattice relaxation times. As a result, pulsed ENDOR can be used in a much larger temperature range provided that an electron spin echo signal can be observed. Two standard ENDOR pulse sequences were introduced by Mims (*2, 3*) in 1965 and Davies (4) in 1974. Along with the rapid developments in pulsed EPR spectroscopy in the past several years (*5–7*), a variety of pulsed ENDOR techniques exists nowadays which are all based on the Mims and Davies pulse sequences. These methods are used to enhance the ENDOR efficiency or to simplify and unravel complicated spectra (*5, 8–10*).

Recently, an increasing interest exists in performing EPR spectroscopy at microwave frequencies much higher than the conventional range of 9–35 GHz. The main advantages are the high spectral resolution and the high absolute sensitivity that can be obtained not only for EPR but also for ENDOR spectroscopy. By using pulsed techniques one adds the advantages of time-resolved operation including the study of transient species. In a number of pulsed ENDOR studies at 95 GHz it was demonstrated that the technique not only works routinely but that it can supply information about systems that cannot be studied with ENDOR techniques at the conventional microwave frequencies for reasons of sensitivity and/or resolution. Examples are a study of the copper site in azurin as well as various paramagnetic centers in silver halides (*11–13*).

In the pulsed ENDOR experiments at 95 GHz the Mims-type ENDOR technique is used. In this method, a $\pi/2-\tau-\pi/2-T-\pi/2$ microwave (MW) pulse sequence, applied resonant with an EPR transition, produces the so-called stimulated echo (SE) at time τ after the third $\pi/2$ MW pulse, as schemetically depicted in Fig. 1. Nuclear transitions are induced by a radiofrequency (RF) pulse, applied between the second and third MW pulses, and can affect the SE intensity. According to the original description given by Mims (*2, 3*) and the more recent operator formalism of Gemperle and Schweiger (*8*), the ENDOR effect must be detected as a decrease of the SE intensity, in agreement with experimental observations so far. Very surprisingly we have discovered that, at low temperatures and a high MW frequency of 95 GHz, the ENDOR effect can also occur as an increase of the SE intensity. An illustration is given in Fig. 2, where part of the ENDOR spectrum of the $S = \frac{1}{2}$ self-trapped hole (STH) complex in AgCl is shown. The spectrum contains nuclear transitions of ^{107}Ag ($I = \frac{1}{2}$, 52%) and ^{109}Ag ($I = \frac{1}{2}$, 48%), and it is seen that the low-frequency transitions occur as an increase of the SE intensity in contrast to their high-frequency counterparts.

In this paper we show that the ''anomalous'' increase of the SE intensity in Mims-type ENDOR can be explained by taking spin–lattice relaxation into account. The description will be given in terms of the operator formalism of Gemperle and Schweiger (*8*) and will be supported by additional ex-

1090-7807/97 $25.00

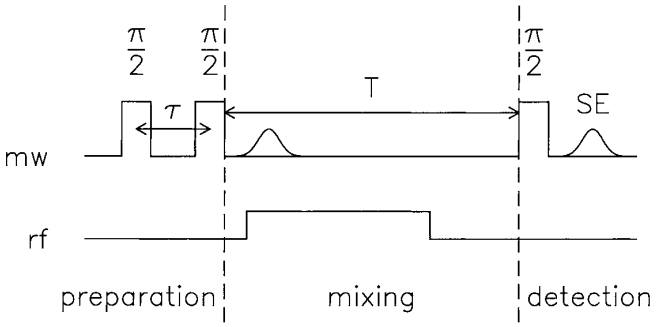

FIG. 1. The Mims-type or stimulated echo microwave pulse sequence. Radiofrequent waves are applied between the second and third $\pi/2$ pulses. The time regions discussed in Section 2 are indicated.

perimental data. An alternative description, based on the method introduced by Mims (*3*), yields identical results and is given elsewhere (*14*). It appears that the effect is most pronounced at high magnetic fields (such as used for 95-GHz EPR spectroscopy) and at low temperature, i.e., at large thermal spin polarizations. The sign of the ENDOR effect is related to the m_s manifold in which the ENDOR transition takes place, and consequently allows for a direct experimental determination of the absolute sign of the hyperfine (HF) interaction. This sign is of importance for the interpretation of the HF interactions but usually must be taken from theoretical considerations. To our knowledge the observation of the anomalous ENDOR effect has not been reported previously, and it presents an additional advantage of performing pulsed ENDOR experiments at high magnetic fields and high microwave frequencies.

2. THEORY

In this section we first review the operator formalism for describing pulsed ENDOR experiments as given by Gemperle and Schweiger (*8*) and apply it to the particular case of the Mims-type ENDOR experiments. We then introduce the effect of spin–lattice relaxation and demonstrate how the ''anomalous'' ENDOR effect develops.

We consider the spin Hamiltonian describing a system consisting of an electron spin $S = \frac{1}{2}$ and one nuclear spin $I = \frac{1}{2}$,

$$H_0 = g_e\beta_e\mathbf{B}_0\cdot\mathbf{S} - g_n\beta_n\mathbf{B}_0\cdot\mathbf{I} + a\cdot\mathbf{S}\cdot\mathbf{I}, \qquad [1]$$

where for simplicity we have taken the g tensor of the electron spin and the hyperfine tensor to be isotropic. In the high magnetic field of the 95-GHz spectrometer, it suffices to replace [1] by the first-order Hamiltonian

$$H_0 = \omega_S S_z + \omega_I I_z + aS_zI_z, \qquad [2]$$

where $\omega_S = g_e\beta_eB_0/\hbar$ and $\omega_I = -g_n\beta_nB_0/\hbar$ represent the electron and nuclear Zeeman frequencies, respectively.

The frequencies of the ($\Delta m_S = 0$, $\Delta m_I = \pm 1$) ENDOR transitions in the two m_s manifolds (α and β states of the electron spin) are given by

$$\omega_{\mathrm{ENDOR}}\left(m_s = \pm\frac{1}{2}\right) = \left(\omega_I \pm \frac{a}{2}\right). \qquad [3]$$

The Hamiltonian describing the effect of the MW and RF pulses is time-dependent. This time dependence is removed by a transformation to a doubly rotating frame by the propagator

$$T = \exp\{-i(\omega_{\mathrm{MW}}tS_z + \omega_{\mathrm{RF}}tI_z)\}, \qquad [4]$$

where ω_{MW} and ω_{RF} represent the angular frequencies of the MW and RF field respectively. In this new frame the Hamiltonian reads as

$$H_0 = \Omega_S S_z + \Omega_I I_z + aS_zI_z, \qquad [5]$$

with $\Omega_S = \omega_S - \omega_{\mathrm{MW}}$ and $\Omega_I = \omega_I - \omega_{\mathrm{RF}}$. The Hamiltonian during the application of the MW pulse is given by

$$H_1 = H_0 + \omega_1 S_x. \qquad [6]$$

Here the second term describes a pulse with a MW field

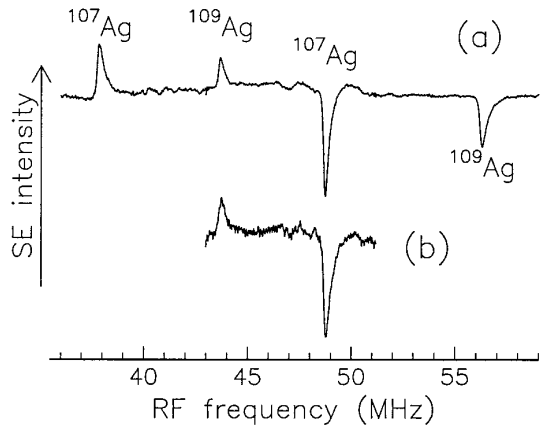

FIG. 2. The ''anomalous'' ENDOR effect observed in the ENDOR spectra of the central silver ion of the self-trapped hole complex ($S = \frac{1}{2}$) in AgCl. Displayed are the ^{107}Ag and ^{109}Ag ENDOR transitions. For the central silver ion, the hyperfine interaction is very large, and the ENDOR transitions appear at frequencies which are separated by two times the nuclear Zeeman splitting (5.5 MHz for ^{107}Ag and 6.25 MHz for ^{109}Ag). The spectra have been obtained at a microwave frequency of 95 GHz and at 1.2 K using the Mims pulse sequence displayed in Fig. 1 ($\tau = 0.5$ μs and $T = 980$ μs (*14*). The magnetic field was parallel to the elongation axis of the STH complex. In (a) and (b) the high-field and the low-field transitions, respectively, are monitored.

strength of $\omega_1 = g_e\beta_e B_1/\hbar = -\gamma_e B_1$ along the x axis of the rotating frame with B_1 the amplitude of the circularly polarized MW field. We assume that the MW pulse is nonselective; i.e., its field strength is much larger than the hyperfine interaction, $|\omega_1| \gg |a|$. This means that all EPR transitions within a spin packet are simultaneously excited by the strong MW pulse. Thus $\omega_1 S_x$ is the dominant term in Eq. [6] and the effect of H_0 can be neglected during the MW pulse.

In contrast to the MW pulse, the RF pulse is selective; i.e., it acts on the nuclear transition either in the $m_s = +\frac{1}{2}$ or in the $m_s = -\frac{1}{2}$ electron spin manifold. The effect of the RF pulse is represented by the Hamiltonians

$$H_2^{\alpha} = \omega_2^E S^{\alpha} I_x,$$

and

$$H_z^{\beta} = \omega_2^E S^{\beta} I_x, \qquad [7]$$

where ω_2^{E} is the hyperfine-enhanced RF field strength (*8*). (In the following we drop the superscript E.)

In all pulsed ENDOR experiments the Hamiltonian in the doubly rotating frame is alternatively constant and time-dependent and can be divided into several periods. The density operator at the end of the sequence is given by

$$\sigma(0) \xrightarrow{H^{(1)}\tau_1} \sigma(\tau_1) \xrightarrow{H^{(2)}\tau_2} \sigma(\tau_1+\tau_2) - - - - \xrightarrow{H^{(n)}\tau_n} \sigma(\sum_n \tau_n). \qquad [8]$$

The observable magnetization components of the electron spin at time $\tau = \Sigma\, \tau_n$ along the x and y axes of the rotating frame can be evaluated from the relations

$$M_x(t) = \mathrm{Tr}\{\sigma(t) S_x\}$$

and

$$M_y(t) = \mathrm{Tr}\{\sigma(t) S_y\}. \qquad [9]$$

The method followed by Gemperle and Schweiger (*8*) is to express the density operator $\sigma(t)$ as a linear combination of base operators

$$\sigma(t) = \sum_n b_n(t) B_n. \qquad [10]$$

In the case of our electron–nuclear two-spin system the complete set $\{B_n\}$ consists of the 16 orthogonal product operators

$$\frac{1}{2}\hat{1}_S\hat{1}_I \quad S_x,\, S_y,\, S_z,\, I_x,\, I_y,\, I_z \quad 2S_xI_x,\, 2S_xI_y,$$
$$2S_xI_z,\, 2S_yI_x,\, 2S_yI_y,\, 2S_yI_z \quad 2S_zI_x,\, 2S_zI_y,\, 2S_zI_z. \qquad [11]$$

The attraction of this method is that it allows for an elegant description of the ENDOR experiments. A pulsed ENDOR experiment starts with the equilibrium state. At 95 GHz and at 1.2 K, in good approximation, only the two low-lying $m_s = -\frac{1}{2}\,(\beta)$ HF levels carry population. The equilibrium state is described by the density operator $\sigma(0) = -S_z + \frac{1}{2}\hat{1}$. Since the unity operator is invariant for the transformations one can take $\sigma(0) = -S_z$ in the absence of relaxation (*8*). However when relaxation is present the unity operator must be included in the following calculations. In the case of nonselective MW excitation in the Mims-type ENDOR experiment (Fig. 2) it can be shown that the $\pi/2-\tau-\pi/2$ pulse sequence during the preparation period leads to an electron nuclear two-spin order term $2S_zI_z$:

$$-S_z + \frac{1}{2}\hat{1} \xrightarrow{(\pi/2)S_x} S_y + \frac{1}{2}\hat{1} \xrightarrow{H_0\tau} \xrightarrow{(\pi/2)S_x}$$
$$S_z\cos[(a/2)\tau]\cos(\Omega_s\tau) - 2S_zI_z\sin[(a/2)\tau]$$
$$\times \sin(\Omega_s\tau) + \frac{1}{2}\hat{1} = \sigma_{\mathrm{prep}}. \qquad [12]$$

The nonselective $\pi/2$ detection pulse applied after the mixing time T generates from σ_{prep} a term S_y which at time $T + 2\tau$ is proportional to the intensity of the stimulated echo

$$\sigma_{\mathrm{prep}} \xrightarrow{(\pi/2)S_x} \xrightarrow{H_0\tau} -S_y\{\cos^2[(a/2)\tau)]$$
$$\times \cos^2(\Omega_s\tau) + \sin^2[(a/2)\tau)]\sin^2(\Omega_s\tau)\}$$
$$= \sigma_{\mathrm{echo}}. \qquad [13]$$

The effect of the RF pulse is to selectively flip the nuclear spin over an angle β_2. An RF pulse on resonance with the nuclear transition $|\alpha\alpha\rangle \leftrightarrow |\alpha\beta\rangle$ in the $m_s = +\frac{1}{2}(\alpha)$ manifold only has an effect on the two-spin order term $2S_zI_z$ in [12] and changes the density operator σ_{prep} (Eq. [12]) into

$$\sigma_{\mathrm{prep}} \xrightarrow{\beta_2 S^{\alpha} I_x} S_z\cos[(a/2)\tau]\cos(\Omega_s\tau)$$
$$-\left\{2S_zI_z\frac{1}{2}(1+\cos\beta_2) - I_z\frac{1}{2}(1-\cos\beta_2)\right\}$$
$$\times \sin[(a/2)\tau]\sin(\Omega_s\tau) + \frac{1}{2}\hat{1} = \sigma_{\mathrm{mix}}^{\alpha}. \qquad [14]$$

The third $\pi/2$ MW pulse, applied after the mixing time T, creates a stimulated echo at time $T + 2\tau$:

$$\sigma^{\alpha}_{\text{echo}} = -S_y\Big\{\cos^2[(a/2)\tau]\cos^2(\Omega_s\tau) + \sin^2[(a/2)\tau]\sin^2(\Omega_s\tau)\,\frac{1}{2}\,(1+\cos\beta_2)\Big\}. \quad [15]$$

A selective RF pulse resonant with the nuclear $|\beta\alpha\rangle \leftrightarrow |\beta\beta\rangle$ transition in the $m_s = -\frac{1}{2}(\beta)$ manifold leads to an expression for σ_{mix} which is almost identical to expression [14]:

$$\sigma^{\beta}_{\text{mix}} = S_z\cos[(a/2)\tau]\cos(\Omega_s\tau) - \left\{2S_zI_z\,\frac{1}{2}\,(1+\cos\beta_2) + I_z\,\frac{1}{2}\,(1-\cos\beta_2)\right\} \times \sin[(a/2)\tau]\sin(\Omega_s\tau) + \frac{1}{2}\,\hat{1}. \quad [16]$$

The third $\pi/2$ microwave pulse applied after the mixing time T again creates an echo $\sigma^{\beta}_{\text{echo}}$ the expression of which is identical to that of $\sigma^{\alpha}_{\text{echo}}$ (Eq. [15]).

It is easily seen from a comparison between Eqs. [13] and [15] that the resonant RF pulse, in the α or β manifold, always leads to a reduction of the echo intensity with a maximum effect at $\beta_2 = \pi$. Further, the reduction of the stimulated echo vanishes if $\sin^2[(a/2)\tau] = 0$ ($\tau = n\cdot 2\pi/a$, $n = 0, 1, 2, \cdots$). This is the well-known ''blind-spot'' effect in pulsed, Mims-type ENDOR (*2, 8*). In what follows we choose, for simplicity, the interval τ between the two $\pi/2$ preparation pulses such that $\tau = \pi/a$; i.e., the S_z-term in Eqs. [14] and [16] is zero and the maximum ENDOR effect is observed upon the application of the RF pulse.

The increase of the intensity of the stimulated echo as observed in Fig. 2 cannot be explained with the model described above. To understand this anomalous increase we must introduce spin–lattice relaxation and study its effect on the expressions for the intensity of the stimulated echo. Since we perform the experiments at 1.2 K and at 95 GHz, the Boltzmann factor $\exp(-\Delta E/kT) \approx 0.02$. Consequently, the relaxation rate Γ from the upper $m_s = +\frac{1}{2}(\alpha)$ to the lower $m_s = -\frac{1}{2}(\beta)$ manifold dominates and we neglect the reverse process (see Fig. 3). We also assume that the spin–lattice relaxation is only effective in the mixing period during time T between the second and third MW pulses. To calculate the effect of the spin–lattice relaxation we must consider the evolution of the diagonal elements of the density matrix, which is described by

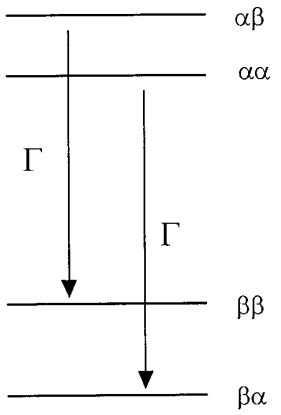

FIG. 3. The spin–lattice relaxation in the $S = \frac{1}{2}$, $I = \frac{1}{2}$ manifold at 95 GHz and 1.2 K.

$$\begin{aligned}
\sigma^{\alpha\alpha}_{\text{mix}}(T) &= \sigma^{\alpha\alpha}_{\text{prep}}\exp\{-\Gamma T\},\\
\sigma^{\alpha\beta}_{\text{mix}}(T) &= \sigma^{\alpha\beta}_{\text{prep}}\exp\{-\Gamma T\},\\
\sigma^{\beta\alpha}_{\text{mix}}(T) &= \sigma^{\beta\alpha}_{\text{prep}} + \sigma^{\alpha\alpha}_{\text{prep}}\{1-\exp(-\Gamma T)\},\\
\sigma^{\beta\beta}_{\text{mix}}(T) &= \sigma^{\beta\beta}_{\text{prep}} + \sigma^{\alpha\beta}_{\text{prep}}\{1-\exp(-\Gamma T)\}. \quad [17]
\end{aligned}$$

This relaxation has an effect on the evolution of σ_{mix}. In the absence of an RF pulse we find after a straightforward calculation using Eqs. [10] and [12], (assuming $\tau = \pi/a$),

$$\sigma_{\text{mix}}(T) = -2S_zI_z\sin(\Omega_s\tau)e^{-\Gamma T} - S_z(1-e^{-\Gamma T}) + \frac{1}{2}\,\hat{1}. \quad [18]$$

Only the first term in [18] contributes to the formation of the stimulated echo, the intensity of which is proportional to

$$\sigma_{\text{echo}} = -S_y\sin^2(\Omega_s\tau)e^{-\Gamma T}. \quad [19]$$

It is seen that the echo intensity, as expected, decays at a rate Γ. Now we apply a $\beta_2 = \pi$ pulse on the ENDOR transition in the $m_s = +\frac{1}{2}(\alpha)$ manifold. We assume that this RF pulse is infinitely short and that it occurs at the start of the mixing period, i.e., immediately after the second MW $\pi/2$ pulse. Then in Eq. [17], $\sigma^{\alpha\alpha}_{\text{prep}}$ must be replaced by $\sigma^{\alpha\alpha,\alpha(\pi)}_{\text{mix}}$ which can be extracted from Eq. [14] with $\tau = \pi/a$. At the end of the mixing period one then finds

$$\sigma^{\alpha(\pi)}_{\text{mix}}(T) = \{-2S_zI_z(1-e^{-\Gamma T}) + I_z\}\sin(\Omega_s\tau) - S_z(1-e^{-\Gamma T}\} + \frac{1}{2}\,\hat{1}. \quad [20]$$

Again only the term with $2S_zI_z$ contributes to the formation of the stimulated echo, the intensity of which is proportional to

$$\sigma_{\text{echo}}^{\alpha(\pi)} = -S_y(1 - e^{-\Gamma T})\sin^2(\Omega_s\tau). \qquad [21]$$

When a $\beta_2 = \pi$ RF pulse is applied on the ENDOR transition in the $m_s = -\frac{1}{2}(\beta)$ manifold, again assuming that this pulse is short and applied immediately after the second MW pulse, we find that

$$\sigma_{\text{mix}}^{\beta(\pi)}(T) = \{-2S_zI_z(e^{-\Gamma T} - 1) - I_z\}\sin(\Omega_s\tau) - S_z(1 - e^{-\Gamma T}) + \frac{1}{2}\hat{1}, \qquad [22]$$

and the stimulated echo is proportional to

$$\sigma_{\text{echo}}^{\beta(\pi)} = -S_y(e^{-\Gamma T} - 1)\sin^2(\Omega_s\tau). \qquad [23]$$

The $\beta_2 = \pi$ RF pulse in either of the two manifolds causes the coefficient of the two-spin order term $2S_zI_z$ in Eqs. [14] and [16] to become equal to zero but the spin–lattice relaxation causes this term to reappear with a sign which depends on the manifold in which the $\beta_2 = \pi$ RF pulse has been applied.

As yet we have only considered the behavior of a single-spin packet. Averaging over all resonance offsets Ω_s with a spectral distribution function $g(\Omega_s) = 1$ (an assumption which is usually fulfilled when the inhomogenous linewidth $\Gamma_{\text{inh}} \gg \omega_1$) makes it possible in expressions [19], [21], and [23] for the echo intensity to replace the term $\sin^2(\Omega_s\tau)$ by $\frac{1}{2}$. Further, it is customary to define an ENDOR efficiency F_{ENDOR} which is a measure for the relative change of the echo amplitude resulting from the RF pulse as

$$F_{\text{ENDOR}} = \frac{1}{2}[I_{\text{echo}}(\text{RF-off}) - I_{\text{echo}}(\text{RF-on})]/I_{\text{echo}}(\text{RF-off}). \qquad [24]$$

In our case where relaxation may cause I_{echo}(RF-off) to become zero we prefer to place in the denominator the value I_{echo}(RF-off, T = 0). According to this definition the ENDOR efficiency F ranges between $0 \leqslant F \leqslant 1$, where $F = 1$ corresponds to an inversion of the SE signal. We thus find in the case of a $\beta_2 = \pi$ RF pulse in the upper $m_s = +\frac{1}{2}(\alpha)$ manifold that

$$F_{\text{ENDOR}}^{\alpha} = \frac{1}{2}(e^{-\Gamma T} - 1 + e^{-\Gamma T}) = \frac{1}{2}(2e^{-\Gamma T} - 1), \qquad [25]$$

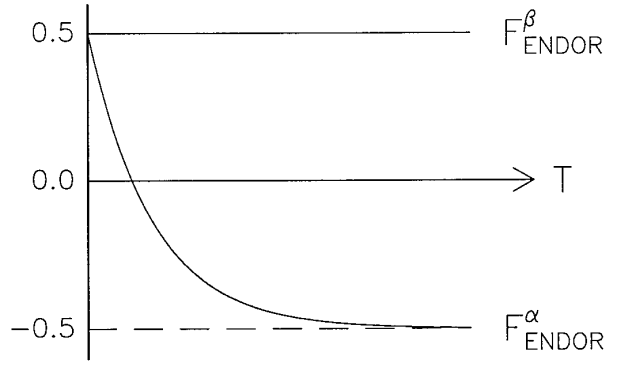

FIG. 4. The time evolution of the ENDOR efficiencies $F_{\text{ENDOR}}^{\alpha}$ and F_{ENDOR}^{β} as defined in Eqs. [25] and [26].

and for a $\beta_2 = \pi$ RF pulse in the $m_s = -\frac{1}{2}(\beta)$ manifold

$$F_{\text{ENDOR}}^{\beta} = \frac{1}{2}(e^{-\Gamma T} - e^{-\Gamma T} + 1) = \frac{1}{2}. \qquad [26]$$

The behavior of the echo efficiencies $F_{\text{ENDOR}}^{\alpha}$ and F_{ENDOR}^{β} is illustrated in Fig. 4. It is seen that F_{ENDOR}^{β} remains positive and constant as a function of T; i.e., it always corresponds to a decrease of the stimulated echo intensity. In contrast $F_{\text{ENDOR}}^{\alpha}$ changes from a positive to a negative value; i.e., for short T it corresponds to a reduction of the SE intensity and for longer T to an increase.

The behavior of the population distribution over the four-level system is illustrated in the diagram presented in Fig. 5. In (a) the effect of spin–lattice relaxation for $T \to \infty$ in the absence of the $\beta_2 = \pi$ RF pulse is shown, whereas in (b) and (c) a $\beta_2 = \pi$ RF pulse is applied in the α or the β manifold respectively. In the figure, it is assumed that $\sin(\Omega_s\tau) = 1$ so that the maximum two-spin order term $2S_zI_z$ has developed during the preparation period. It is seen that for long T, opposite two-spin order terms $2S_zI_z$ develop upon the application of the $\beta_2 = \pi$ RF pulse either in the α or in the β manifold. The negative term $-2S_zI_z$ leads to an increase of the SE intensity and the positive term $2S_zI_z$ to a decrease (in the limit $T \to \infty$ to a SE echo with opposite phase).

3. EXPERIMENTAL

The predicted behavior of the change in the SE intensity upon excitation in the $m_s = +\frac{1}{2}(\alpha)$ and $m_s = -\frac{1}{2}(\beta)$ manifold is nicely illustrated by pulsed Mims-type ENDOR experiments on the self-trapped hole (STH) complex in AgCl (*14*). This hole is created in the AgCl crystal upon ultraviolet irradiation and is trapped on a $AgCl_6$ unit that has undergone a Jahn–Teller distortion along a cubic axis. The orbital angular momentum of this hole is almost quenched, and we

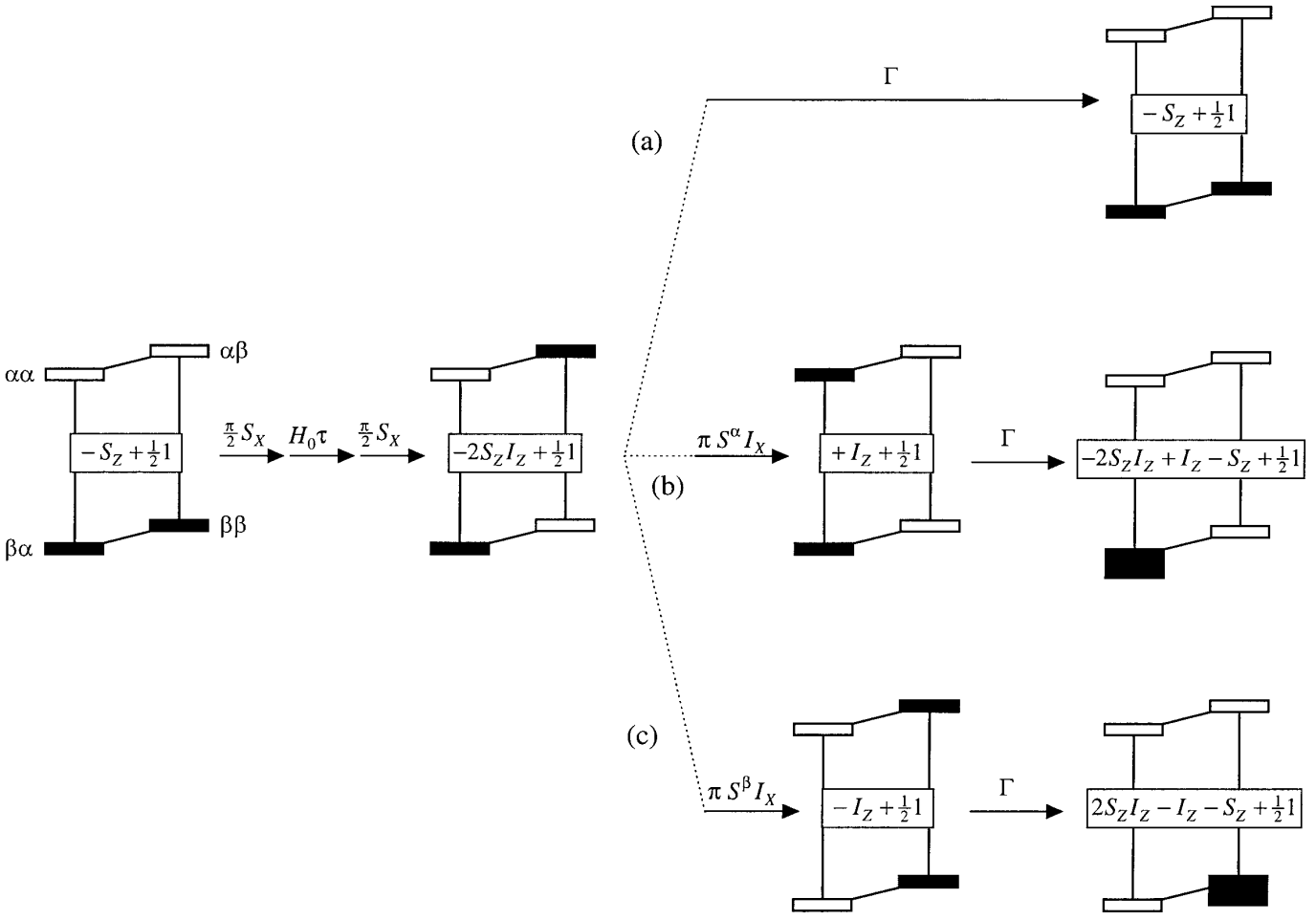

FIG. 5. The behavior of the population distribution over the four-level system. In (a) the effect of spin–lattice relaxation in the absence of RF pulses is indicated. In (b) and (c) a $\beta_2 = \pi$ RF pulse in the α and β manifold, respectively, is applied. We have used $\sin(\Omega_s\tau) = 1$ and $\sin[(a/2)\tau] = 1$ so that the maximum two-spin order term $2S_zI_z$ has developed upon the application of the two $\pi/2$ MW preparation pulses. In the last column the population distribution is shown for $T \to \infty$.

deal with an effective $S = \frac{1}{2}$ electronic system. The ^{107}Ag and ^{109}Ag ENDOR resonances of the silver ions surrounding the central $AgCl_6$ unit of the STH can be observed using the Mims technique at 95 GHz and at T = 1.2 K. In Fig. 6, the results are presented with an interval $\tau = 0.35$ μs between the two MW preparation pulses and for various values of T. The length of the RF pulse is not infinitely short because of lack of RF power and is kept 10 μs shorter than T. Nevertheless the results show the effect of spin–lattice relaxation by the evolution of the ENDOR signal, which follows a behavior as predicted by Eqs. [25] and [26]. It is seen that the sign of the ENDOR transitions of the two silver isotopes below their respective Zeeman frequencies is negative; i.e., the signals correspond to a reduction of the SE intensity, independent of T. In contrast, the high-frequency ENDOR transitions are weak and negative for short values of T and turn over to a positive value, corresponding to an increase of the SE intensity, for long values of T in agreement with the prediction of Eq. [25].

The observation of the anomalous ENDOR effect for the STH allows us to derive the sign of the hyperfine interaction. As the ENDOR frequency of the $S = \frac{1}{2}$ unpaired spin of the STH with a $I = \frac{1}{2}$ silver nucleus amounts in first order to

$$\nu_{\mathrm{ENDOR}}\left(m_s = \pm\frac{1}{2}\right) = \frac{1}{h}\left|g_n\beta_nB_0 \mp \frac{1}{2}a\right|,$$

where $g_n(\mathrm{Ag}) < 0$, it follows from the findings in Fig. 6 that the superhyperfine interaction between the hole and the silver nuclei must have a positive sign. An ENDOR study of the self-trapped exciton in AgCl (*13*) confirms in an independent manner the sign thus obtained. Also according to our model the ''anomalous'' ENDOR effect

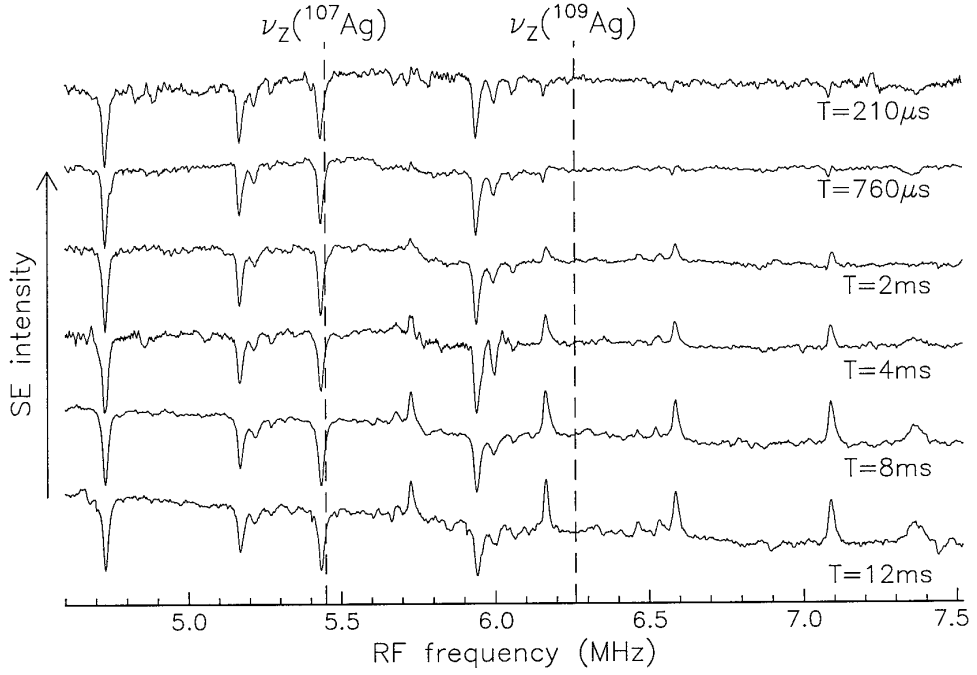

FIG. 6. The effect of spin–lattice relaxation on the intensity of the SE echo in the case of Mims-type ENDOR experiments. The spectra contain ^{107}Ag and ^{109}Ag ENDOR transitions of silver ions surrounding the central $AgCl_6$ unit of the STH complex in AgCl and have been recorded at 1.2 K and at 95 GHz with the magnetic field parallel to the D_{4h} distortion axis of the complex. The interval between the $\pi/2$ MW preparation pulses $\tau = 0.35$ μs and the RF pulse length is taken to be 10 μs shorter than the values of T listed. In addition we have indicated the values of the Zeeman frequencies of ^{107}Ag and ^{109}Ag by $\nu_z(^{107}Ag)$ and $\nu_z(^{109}Ag)$, respectively.

should appear when $(2e^{-\Gamma T} - 1) < 0$ which, with the low-temperature value of $\Gamma = [(10 \pm 2)\ \text{ms}]^{-1}$ of the STH (*14*), would require that $T > (7 \pm 1)$ ms. It is remarkable that, despite the simplifications in our model, this estimate agrees with the time scale at which the anomalous lines appear in Fig. 6.

It is important to realize that the anomalous ENDOR effect only develops in the case of large thermal spin polarizations such as encountered in our experiments at 1.2 K and at 95 GHz. Inspection of Fig. 5 shows that the relaxation, creating the two-spin order term $2S_zI_z$, only occurs between the two levels $|\alpha\alpha\rangle \leftrightarrow |\beta\alpha\rangle$ (case b) and $|\alpha\beta\rangle \leftrightarrow |\beta\beta\rangle$ (case c), and not between the other two levels because they are empty (in good approximation). At small Boltzmann factors, such as encountered at 9 GHz, the other two levels carry a population which is only slightly different, and spin–lattice relaxation between them counteracts the effect of the first two levels on the term $2S_zI_z$.

4. CONCLUSION

A description of Mims-type ENDOR for a $S = \frac{1}{2}$, $I = \frac{1}{2}$ electron spin, nuclear spin system is presented using the operator formalism developed by Gemperle and Schweiger and including the effect of spin–lattice relaxation. We have considered only downward relaxation from the upper $m_s = +\frac{1}{2}$ spin manifold toward the lower $m_s = -\frac{1}{2}$ manifold in the limit of a large thermal spin polarization as it applies for experiments performed at 95 GHz and at 1.2 K. The model can explain the observation of the anomalous increase of the stimulated echo intensity upon the application of the RF pulse. It is shown that this anomalous increase points to ENDOR transitions in the upper $m_s = +\frac{1}{2}$ manifold, and consequently it makes it possible to determine the sign of the hyperfine interaction. It is argued that the effect can only be observed at large thermal spin polarizations, and it presents another advantage of EPR/ENDOR spectroscopy at high microwave frequencies.

ACKNOWLEDGMENTS

The work forms part of the research programs of the ''Stichting voor Fundamenteel Onderzoek der Materie FOM'' and of the ''Stichting Scheikundig Onderzoek Nederland SON'' with financial support from the ''Nederlandse Organisatie voor Wetenschappelijk Onderzoek NWO.''

REFERENCES

1. G. Feher, *Phys. Rev.* **103,** 834 (1956).
2. W. B. Mims, *Proc. R. Soc. London A* 283 (1965).
3. W. B. Mims, *in* ''Electron Paramagnetic Resonance'' (S. Geschwind, Ed.), p. 344, Plenum Press, New York (1972).
4. E. R. Davies, *Phys. Lett. A* **47,** 1 (1974).

5. A. Schweiger, *J. Chem. Soc. Faraday Trans.* **91,** 177 (1995).
6. A. Schweiger, *Angew. Chem. Int. Ed. Engl.* **30,** 265 (1991).
7. J. H. Freed, *J. Chem. Soc. Faraday Trans.* **86,** 3173 (1990).
8. C. Gemperle and A. Schweiger, *Chem. Rev.* **91,** 1481 (1991).
9. G. Jeschke and A. Schweiger, *J. Chem. Phys.* **103,** 8329 (1995).
10. G. Jeschke and A. Schweiger, *Chem. Phys. Lett.* **246,** 431 (1995).
11. M. T. Bennebroek, O. G. Poluektov, A. J. Zakrzewski, P. G. Baranov, and J. Schmidt, *Phys. Rev. Lett.* **74,** 442 (1995); M. T. Bennebroek, A. Arnold, O. G. Poluektov, P. G. Baranov, and J. Schmidt, *Phys. Rev. B* **54,** 11276 (1996).
12. J. W. A. Coremans, M. van Gastel, O. G. Poluektov, E. J. J. Groenen, T. den Blaauwen, G. van Pouderoyen, G. W. Canters, H. Nar, C. Hamman, and A. Messerschmidt, *Chem. Phys. Lett.* **235,** 202 (1995).
13. M. T. Bennebroek, A. Arnold, O. G. Poluektov, P. G. Baranov, and J. Schmidt, *Phys. Rev. B* **53,** 15607 (1996).
14. M. T. Bennebroek, Thesis, University of Leiden 1996, Chaps. 2 and 4.